



## Analyzing DBH estimation accuracy and ecological influences across size classes using SLAM LiDAR and RANSAC algorithm in Korean Forests

Kim Daeyeol, Noh Jaesang, Kelvin Kang, Yeon Young-Kwang & Shin Wonhyeop

**To cite this article:** Kim Daeyeol, Noh Jaesang, Kelvin Kang, Yeon Young-Kwang & Shin Wonhyeop (2025) Analyzing DBH estimation accuracy and ecological influences across size classes using SLAM LiDAR and RANSAC algorithm in Korean Forests, International Journal of Remote Sensing, 46:22, 8762-8783, DOI: [10.1080/01431161.2025.2572045](https://doi.org/10.1080/01431161.2025.2572045)

**To link to this article:** <https://doi.org/10.1080/01431161.2025.2572045>



Published online: 21 Oct 2025.



Submit your article to this journal [↗](#)



Article views: 36



View related articles [↗](#)



View Crossmark data [↗](#)



# Analyzing DBH estimation accuracy and ecological influences across size classes using SLAM LiDAR and RANSAC algorithm in Korean Forests

Kim Daeyeol<sup>a</sup>, Noh Jaesang<sup>b</sup>, Kelvin Kang<sup>c</sup>, Yeon Young-Kwang<sup>d</sup> and Shin Wonhyeop<sup>a</sup>

<sup>a</sup>InvaLab Inc., Research and Development, Siheung-si, Gyeonggi-do, Republic of Korea; <sup>b</sup>Climate Change Adaptation Team, National Institute of Ecology, Geumgang-Ro, Seochen-Gun, Republic of Korea; <sup>c</sup>UCS Co, Yeongtong-gu, Suwon-Si, Gyeonggi-do, Republic of Korea; <sup>d</sup>Korea Institute of Geoscience and Mineral Resources, Gyeonggi, Daejeon, Republic of Korea

## ABSTRACT

Simultaneous Localization and Mapping (SLAM) Light Detection and Ranging (LiDAR) technology is a powerful option for forest inventory, particularly for estimating tree Diameter at Breast Height (DBH). However, the variability in DBH-estimation accuracy across different size classes and ecological conditions remains underexplored. We therefore assessed a handheld SLAM LiDAR workflow in three ecologically distinct Korean forests – *Quercus mongolica* on Namsan, *Pinus densiflora* on Jeombongsan, and a mixed *Quercus* stand on the same mountain – selected to span gradients in elevation, canopy density, and species composition. Point clouds acquired with an Ouster OS1-32 sensor (650 k pts s<sup>-1</sup>, 30 mm accuracy, 120 m range) were geo-referenced with ground-control points, denoised, and processed with a Random Sample Consensus (RANSAC) cylinder-fitting algorithm to derive DBH. LiDAR-derived DBH corresponded closely to field measurements ( $R^2 = 0.98$ , RMSE = 1.84 cm, MAE = 1.45 cm, maximum error = 4.35 cm). Measurement reliability increased sharply above a threshold of 23.5 cm, whereas trees with DBH under 10 cm exhibited the largest deviations (MAPE = 30.76%; rRMSE = 33.71%). Accuracy peaked for larger trees, with  $R^2$  reaching 0.96 in the 40 cm class. Shade-tolerant species such as *Acer pseudosieboldianum* and *Styrax japonicus*, which often have curved stems, showed greater variability, whereas canopy-dominant *Quercus mongolica* and *Pinus densiflora* displayed uniform growth and lower error. These discrepancies in small-diameter trees are likely due to the limited number of LiDAR points captured and the stronger influence of competitive growth, as non-upright stems can introduce errors in both LiDAR and manual measurements.

## ARTICLE HISTORY

Received 17 February 2025  
Accepted 3 October 2025

## KEYWORDS

DBH; forest management; 3D mapping; RANSAC; stem diameter Forest Inventory

## 1. Introduction

Trees are vital components of forest ecosystems, serving as essential carbon sinks and contributing significantly to forest inventory, carbon cycle modelling, and habitat assessments (Huang et al. 2011; Kirby and Potvin 2007). Among the measurable tree growth

metrics, Diameter at Breast Height (DBH) is critical for estimating aboveground biomass, a key metric in understanding forest carbon dynamics and ecosystem health. DBH can explain up to 95% of biomass variability, with accuracy enhanced by incorporating parameters like tree height and wood density (Aabeyir, Kyereh, and Anaba 2020; Baker et al. 2004; Nam et al. 2016; Parresol 1999). Additionally, DBH measurements offer insights into tree age, structural dynamics, and stand competition, providing a comprehensive understanding of forest development over time. This parameter not only reflects the current state of individual trees but also serves as a reliable indicator of overall forest health and productivity, which is crucial for modelling long-term ecological trends (Compeán-Aguirre et al. 2024).

The advent of Light Detection and Ranging (LiDAR) technology has transformed forest inventory by enabling high-resolution surveys of forest resources, carbon stocks, and biodiversity at larger scales (McRoberts, Tomppo, and Næsset 2010; Tomppo et al. 2010). LiDAR's ability to generate detailed 3D representations of forest structures has made it indispensable for modern ecological studies. Among various LiDAR systems, Simultaneous Localization and Mapping (SLAM) LiDAR stands out for its portability and ability to collect detailed 3D spatial data in real time, particularly useful in complex and dense forest terrains (Aschoff and Spiecker 2004). Unlike airborne LiDAR systems, SLAM LiDAR allows for ground-level measurements with minimal logistical constraints, making it highly adaptable to diverse forest environments. The high-resolution point clouds generated by SLAM LiDAR have proven effective in characterizing both individual tree structures and larger forest landscapes, enabling enhanced accuracy in ecological modelling, biomass estimation, and habitat assessments (Yang et al. 2024). These capabilities underscore its potential for addressing complex challenges in forest management, such as monitoring species-specific growth trends and assessing carbon sequestration dynamics. Furthermore, the cost-effectiveness of SLAM LiDAR compared to other remote sensing technologies makes it particularly attractive for large-scale forest surveys in resource-limited settings (Pang, Zhou, and Huang 2024). Compared to other ground-based laser scanning systems, SLAM-based LiDAR offers unique advantages in forest environments. While Mobile Laser Scanning (MLS) provides efficient data acquisition over broad areas and Terrestrial Laser Scanning (TLS) yields the highest accuracy in static plots, SLAM systems excel in GNSS-denied and complex terrains due to their real-time mapping capabilities and operational flexibility (Bienert et al. 2018; Balestra et al., 2024; Shao et al. 2020). However, trade-offs exist among these approaches, particularly in terms of point density and acquisition constraints. TLS achieves high precision with RMSE values below 1 cm for DBH estimation, whereas MLS offers reasonable accuracy but tends to struggle with finer structural details. SLAM-based systems, despite being more susceptible to occlusion or drift errors, have demonstrated competitive DBH accuracy – reporting estimation errors below 5 cm under optimized processing conditions (Guan et al. 2024). These comparisons underscore the need for sensor-specific calibration when deploying SLAM LiDAR in forest inventory applications.

SLAM LiDAR applies the Random Sample Consensus (RANSAC) algorithm to estimate DBH by fitting cylindrical shapes to point cloud data. This approach is particularly effective in mitigating noise and occlusion, which are common challenges in forested areas (Schnabel, Wahl, and Klein 2007). Despite its strengths, RANSAC has certain limitations, including reduced accuracy for smaller DBH trees due to sparse point cloud density and

irregular growth forms. For instance, slender or non-cylindrical stems often produce higher errors as RANSAC struggles to accurately fit geometric primitives under these conditions (Morales and MacFarlane 2024). Recent studies have compared RANSAC with other state-of-the-art algorithms for DBH estimation, highlighting its robustness and efficiency in various conditions (Xie et al. 2020; Yao, Krzystek, and Heurich 2012). However, these comparisons also underscore gaps, such as its performance in capturing finer structural details or adapting to heterogeneous ecological conditions. Emerging alternatives, including machine learning-based methods, offer potential improvements, yet RANSAC remains widely used due to its computational simplicity and effective performance in diverse forest environments. These advantages, combined with its flexibility in varying ecological contexts, continue to position RANSAC as a valuable tool in forest monitoring applications (Salehi, Jarahizadeh, and Sarafraz 2022).

Existing research has highlighted several limitations in SLAM LiDAR-based DBH estimation. Notably, inaccuracies in smaller DBH classes remain a persistent challenge, often leading to the underestimation of forest biomass and structural complexity. While individual small-diameter trees contribute relatively little biomass, their high frequency within forest stands can significantly impact total estimates if excluded. Prior studies have demonstrated that omitting small-diameter trees from inventories can lead to biomass underestimations of up to 30% in certain forest types (Haripriya 2002; Nalaka, Sivananthawerl, and Iqbal 2013). Moreover, inaccuracies in these small-diameter classes are not always limited to underestimation; several recent studies have reported systematic overestimation arising from partial stem coverage, occlusion effects, or circle-fitting bias under low point densities (Kuželka and Surový 2024; Pierzchała, Giguère, and Astrup 2018; Xie et al. 2022). These bidirectional errors underscore the need for more precise evaluations of SLAM-based DBH estimation, particularly with respect to error direction and magnitude across different DBH ranges.

Additionally, while previous studies have visualized DBH estimation models, they have often lacked comprehensive evaluations of ecological implications, particularly regarding species-specific growth patterns and competition dynamics (Zhao, Popescu, and Nelson 2009). Understanding the specific DBH intervals where inaccuracies occur is critical for refining methodologies and improving accuracy. These refinements should address practical ecological challenges, including ensuring measurement accuracy across diverse forest types and improving the adaptability of DBH models to specific conditions. Enhanced calibration models tailored to unique forest characteristics can mitigate these issues, making SLAM LiDAR a more reliable tool for diverse environmental applications (Liu et al. 2021; Xie et al. 2022). While recent studies have explored advanced 3D tree modelling techniques using hierarchical or matrixial representations to reconstruct full tree morphology (Kurdi et al. 2024; Tarsha-Kurdi et al. 2024), these approaches have primarily focused on structural visualization rather than precise DBH quantification. In contrast, our study emphasizes the evaluation of SLAM-based DBH estimation accuracy across varying ecological and structural conditions, contributing directly to methodological improvements for forest inventory.

We extend earlier work by analysing error distributions not only across DBH intervals but also across dominant species groups, providing an initial link between measurement error, growth form, and competitive status. The study identifies the conditions where inaccuracies are most prominent and examines how

environmental factors, species variability, and point cloud density influence measurement precision. The proposed approach offers actionable insights for improving SLAM LiDAR-based forest monitoring and ensuring its alignment with real-world ecological needs.

This study focuses on three primary objectives:

- (1) To evaluate the accuracy of SLAM LiDAR in estimating DBH across different size classes and forest conditions, as part of ongoing efforts to assess its applicability in forest measurement.
- (2) To identify the DBH intervals where SLAM LiDAR-based estimates are prone to inaccuracies and examine relevant patterns observed in the results.
- (3) To assess the ecological implications of DBH estimation inaccuracies and consider potential approaches to mitigate their effects on forest monitoring and management practices.

By addressing these objectives, this research aims to build a clearer basis for applying SLAM LiDAR in forest inventory, with the goal of improving the accuracy and ecological relevance of forest monitoring efforts. The results are intended to refine existing methodological approaches and provide field-applicable insights to support effective forest monitoring and management.

## 2. Materials and methods

### 2.1. Study area

This study was conducted in permanent forest monitoring plots established by the National Institute of Ecology (NIE) in Korea, which were classified based on the dominant tree species present in the area: NQ and JQ plots were dominated by *Quercus mongolica*, while the JP plot represented a forest of *Pinus densiflora*. The NQ plot is situated on the summit slope of Namsan in Seoul, encompassing a total area of 1,600 square metres (40 metres by 40 metres), and field data for this plot was collected on 7 March 2024. The JP plot, located on the northern slope of Jeombongsan in Gangwon-do, covers a larger area of 2,500 square metres (50 metres by 50 metres), with data acquisition completed on 26 April 2024. The JQ plot consists of three smaller subplots, each measuring 400 square metres (20 metres by 20 metres), and together they form a total area of 1,200 square metres; field surveys for the JQ plot were conducted on 25 April 2024 ([Figure 1](#)).

According to long-term forest monitoring data maintained by the NIE, the NQ, JP, and JQ plots contain 232, 517, and 230 individual trees of canopy species – defined in this study as tree species that reach or contribute to the uppermost forest layer in mature stands – respectively (National Institute of Ecology [2023](#)).

Although it is technically possible to scan and measure all trees within a 50 × 50 m plot, we limited the sample to 60 canopy trees per plot to ensure consistent sampling across sites with different tree densities. This number was chosen to represent a broad range of DBH values while allowing an even spatial distribution. In the field, reference measurements were collected along paths planned to pass near the selected trees, enabling efficient and balanced coverage across each plot.

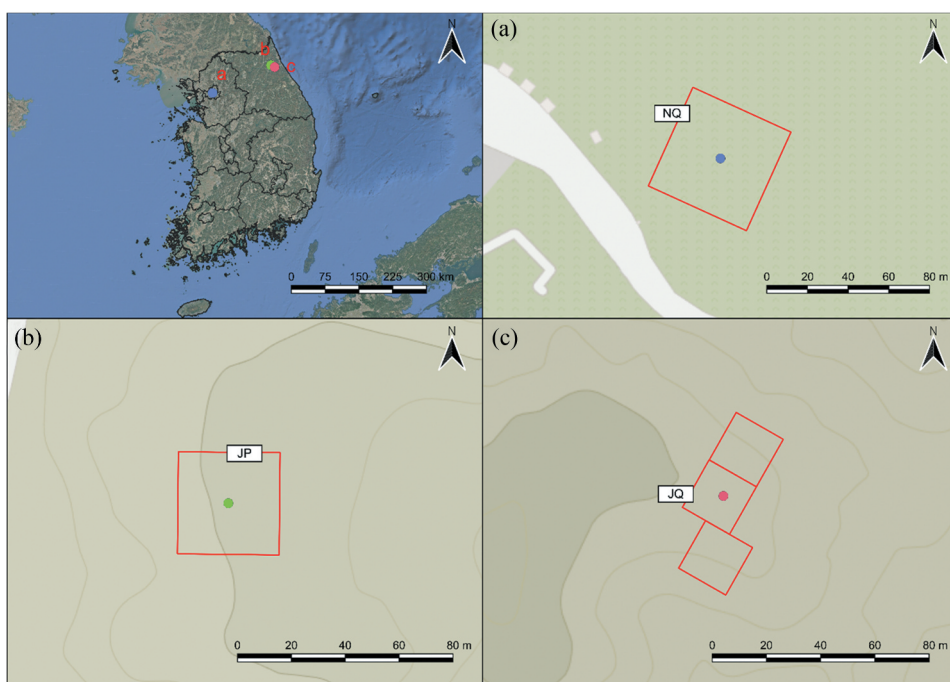


**Figure 1.** Location of study sites in Korea. (a) NQ refers to the *Quercus mongolica* forest located at Namsan, (b) JP refers to the *Pinus densiflora* forest located at Jeombongsan, and (c) JQ refers to the *Quercus mongolica* forest located at Jeombongsan.


## 2.2. Data acquisition

SLAM LiDAR scanning was performed at all three study locations – Namsan in Seoul and the two Jeombongsan sites (*Quercus mongolica* and *Pinus densiflora* forests) – to ensure a thorough capture of forest structure and reduce errors arising from scanning inconsistencies. At each site, four separate scans were conducted using the uMaps-32 SLAM LiDAR system, which integrates the Ouster OS1-32 sensor (Ouster Inc., U.S.A.). This sensor is capable of capturing 650,000 points per second, with a scanning accuracy of  $\pm 30$  millimetres and a maximum effective range of 120 metres (Table 1). The system processes laser points to detect and record the locations of distinct features in three dimensions, utilizing odometry measurements to construct a precise 3D spatial map of the scanned area.

During data collection, the LiDAR sensor was positioned 30 centimetres above the operator's head to minimize obstruction by branches and vegetation. The device was tilted at multiple angles in areas with limited foliage to ensure accurate scanning of the tree canopy and to reduce shadowed regions caused by variations in terrain and vegetation height. At each study site, 60 trees were selected, covering a DBH range of 3 to 55 centimetres, and were labelled with high-contrast numbers ranging from 1 to 60 to facilitate their identification during LiDAR scanning (see Appendix, Figs. A1–A3 for SLAM scan trajectories). The trees were evenly distributed along the SLAM LiDAR path to ensure comprehensive spatial coverage. The nominal point density across the three study sites averaged  $5,945 \text{ pts m}^{-2}$ , based on total point counts and horizontal scan areas. Individually, the NQ, JP, and JQ plots exhibited densities of  $9,060$ ,  $4,718$ , and  $4,057 \text{ pts m}^{-2}$ , respectively.



**Table 1.** Specifications of uMaps-32 Mobile SLAM LiDAR.

Specifications of uMaps-32 Mobile SLAM LiDAR	
	Sensor: Ouster OS1-32
	Max.Range: ≤120m at 80% reflectivity
	Typical Range Accuracy : ± 30 mm
	Beam Divergence: 0.18°(3 mrad)
	Beam footprint : 22 cm at 100 m
	Scanning channels/beams: 32 channels
	Output rate : 655,360 pts s <sup>-1</sup>
	Laser Returns: 1 per outgoing pulse
	FOV (Vertical) : 45°(± 22.5°)
	Rotation Rate : 10 - 20 Hz
	Angular resolution: 0.35°-2.8°
	Operating Temperature : -20 to +50°C

To improve geographic accuracy and enhance the reliability of the collected data, five to six Ground Control Points (GCPs) were established at strategically important locations within each study site for georeferencing the SLAM LiDAR scans. DBH measurements were taken manually using a caliper, and the values were calculated as the average of the long and short diameters. Additionally, the x, y, and z coordinates of each sampled tree were recorded using the KMapper software (2024 version), which applies advanced filtering techniques to stabilize positional data and calculates mean sea level altitude for precise identification of tree locations. The incorporation of GCPs and the manually measured DBH values played a critical role in validating the DBH estimates derived from the SLAM LiDAR data.

**2.3. Data processing and georeferencing**

The initial stage of LiDAR data processing involved terrain normalization, which serves as a foundational step for consistent DBH estimation and further structural analysis (McRoberts, Tomppo, and Næsset 2010). Raw point cloud data was extracted from the SLAM equipment’s Bag files, which contained both 3D point coordinates and trajectory metadata. Trajectory alignment was corrected using custom Python scripts implemented with the Open3D library, ensuring spatial consistency and accuracy across scan sequences. The corrected data was then exported to the PLY format for further processing and visualization.

To classify terrain surfaces, we applied the Cloth Simulation Filtering (CSF) algorithm (Zhang et al. 2016) using CloudCompare, an open-source point cloud processing software. This method performs ground versus non-ground classification by simulating a cloth-like mesh that drapes over the point cloud to distinguish ground points from above-ground features such as vegetation and tree trunks. The algorithm was parameterized with a cloth resolution of 0.3 and a classification threshold of 0.1 metres. For sloped terrains, these parameters were tuned to minimize ground point misclassification and ensure accurate surface extraction.

After ground point classification, a Digital Elevation Model (DEM) was generated at a spatial resolution of 0.1 metres using raster interpolation techniques consistent with the methodology of Zhou et al. (2021). Point cloud normalization was subsequently performed using PDAL, aligning the z-values of all points to the ground surface. This normalization ensured that DBH-related calculations were consistently referenced at 1.2 metres above ground level across all plots.

Finally, statistical filtering was applied to remove outlier points that deviated significantly from the local surface profile. Specifically, a 0.5-metre search radius and a standard deviation threshold of 1.0 were used to identify and eliminate noise, thereby enhancing the structural clarity and overall reliability of the dataset (workflow illustrated in Figure 2).

2.4. Individual tree parameter estimation

To estimate tree parameters from the LiDAR dataset, we combined field-measured data with a RANSAC-based cylinder-fitting algorithm (Figure 3). The algorithm models each trunk as a series of cylindrical cross-sections using points captured within the designated

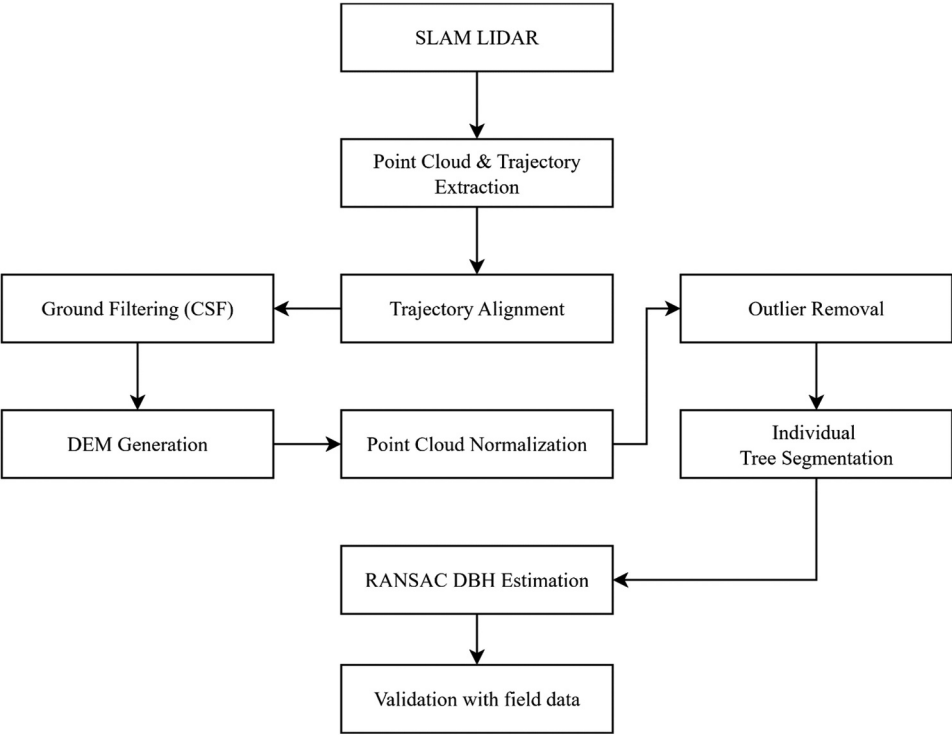


**Figure 2.** Workflow of SLAM LiDAR data processing and DBH estimation. The flowchart illustrates the data processing pipeline, beginning with the extraction of point cloud and trajectory data from SLAM LiDAR devices. Ground points are identified using cloth Simulation Filtering (CSF) followed by DEM generation. In parallel, outlier points are removed before individual tree segmentation. All data are normalized relative to ground elevation and used to estimate tree DBH through a RANSAC-based cylinder fitting method. The final estimates are validated against field-measured tree parameters.



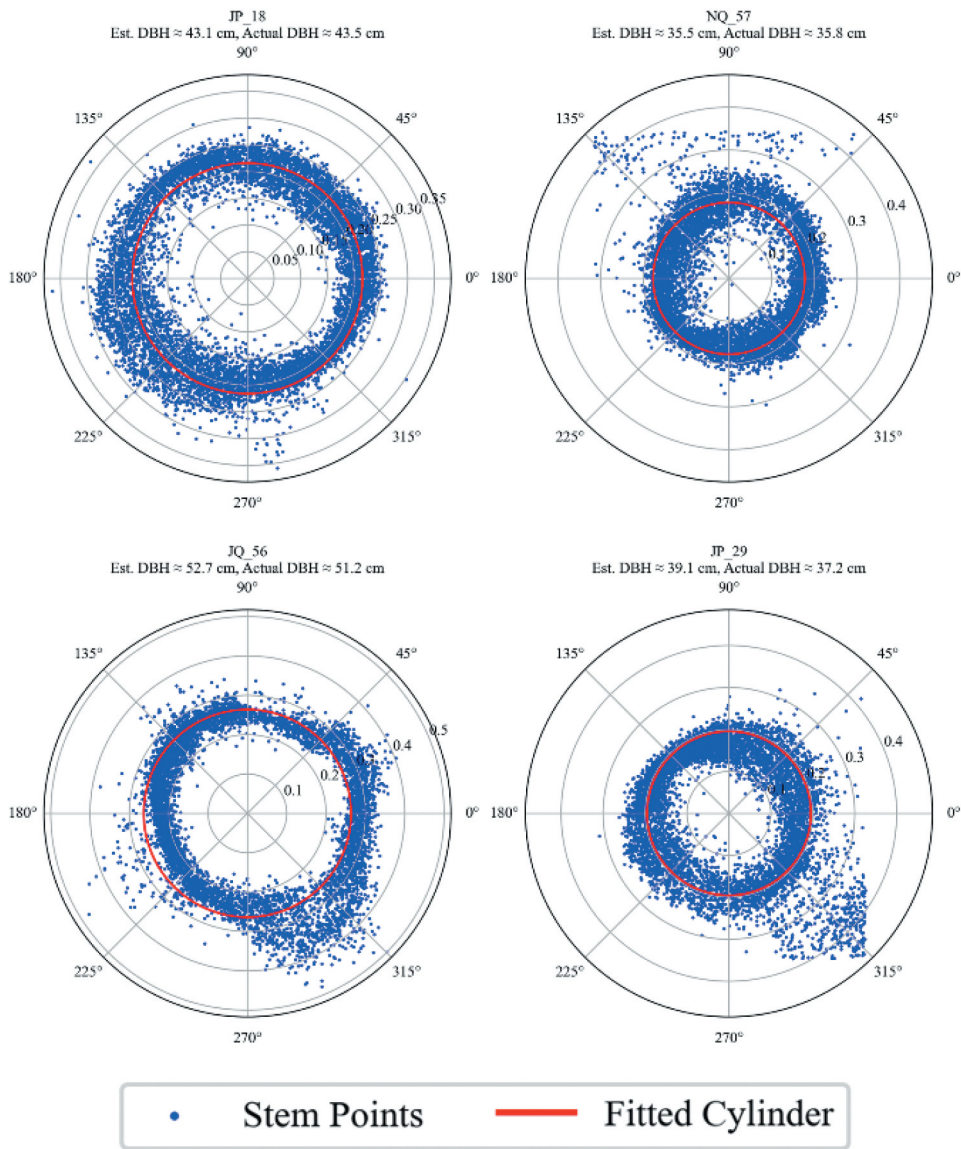


**Figure 3.** Estimation of DBH using a RANSAC-based cylinder-fitting algorithm. Individual tree trunks were identified and extracted based on seed points within a DBH height range of 1.2–1.4 meters. GPS x, y, and z coordinates recorded during fieldwork were used to accurately position each tree in the LiDAR dataset.

DBH height band (1.2–1.4 m above ground level). RANSAC iteratively identifies inlier points that best represent the trunk surface while discarding outliers.

The RANSAC procedure was first calibrated for tree-trunk modelling. A grid search was conducted on a validation subset of 30 reference trees, testing residual thresholds of 0.005–0.020 m (0.002 m increments), iteration counts of 100–1 000 (step 100), Z tolerances of 0.10–0.20 m (step 0.02 m), and XY tolerances scaled from

1.0 to  $1.4 \times (\text{DBH} / 2)$  in 0.1-step increments. A residual threshold of 0.01 m and 500 iterations gave the most stable fits and the lowest absolute DBH deviations across species and stem sizes, and were therefore adopted for the full dataset. The Z tolerance was fixed at 0.15 m, while the XY tolerance remained dynamically scaled to  $1.2 \times (\text{DBH} / 2)$  to focus on the expected trunk radius and exclude surrounding clutter. A circular-cylinder model was retained because Ye et al. (2020) showed that cylinder fitting achieved the lowest DBH RMSE among the geometric models they evaluated.

DBH estimates derived from the fitted cylinders were validated against field-measured DBH values. Accuracy and reliability were quantified with the coefficient of determination ( $R^2$ ) and the mean absolute error (MAE). Tree height was estimated separately by analysing LiDAR points within a 2.5 m radius of each stem and selecting the 95th percentile of point elevations, a procedure that mitigates the influence of outliers and yields robust height measurements.

## 2.5. Manual tree species identification

Tree species identification was performed for a representative sample of individuals during the LiDAR survey. Plant specialists from the National Institute of Ecology (NIE) determined each stem's species in the field while DBH was being measured, consulting the National List of Species of Korea (National Institute of Biological Resources 2023) and the Coloured Flora of Korea (Lee, 2003) for scientific names. In post-processing, all stems whose trunks intersected the SLAM trajectory were reviewed, producing a verified subset that encompassed every species observed in the field, for a total of 31 species.

## 2.6. Statistical analysis

Statistical analyses were conducted to explore the relationships between various tree parameters and to ensure the robustness of the study's findings. The Height to DBH Ratio (HDR), which quantitatively represents tree form by relating tree height to DBH, was analysed to evaluate variations among individuals and species. To meet the assumptions of parametric tests, HDR values were Box-Cox transformed to achieve normality (Shapiro-Wilk test:  $W = 0.987$ ,  $p = 0.11$ ). The transformed data were then subjected to a one-way ANOVA, followed by Tukey's Honestly Significant Difference (HSD) post hoc test, to compare DBH groups and identify significant differences between them.

All statistical analyses were performed using R version 4.4.1 (R Core Team 2024). During the analysis, it was observed that one tree sampled in the Namsan plot was a broken, dead individual. As its inclusion would have introduced significant inaccuracies into both ecological and statistical interpretations, this tree was excluded from the dataset. Although the tree was known to be dead at the time of field measurement, it was retained for DBH accuracy evaluation, as both manual and LiDAR-based measurements were successfully conducted. However, it was excluded from analyses involving species composition, HDR, and other ecological interpretations to prevent bias arising from non-living individuals.

### 3. Results

#### 3.1. DBH accuracy in LiDAR and field measurements

SLAM LiDAR-based DBH measurements were validated against manual field measurements across three study sites – NQ, JQ, and JP – using key statistical metrics such as Mean Absolute Error (MAE), Mean Absolute Percentage Error (MAPE), Root Mean Squared Error (RMSE), and relative Root Mean Squared Error (rRMSE). The results demonstrated a strong agreement between LiDAR-derived and manual measurements, as summarized in [Table 2](#).

Among the three sites, NQ exhibited the highest accuracy, with an MAE of 1.0 cm and the highest  $R^2$  value of 0.99. This near-perfect alignment between LiDAR and manual DBH measurements can be attributed to the uniform canopy structure and minimal undergrowth, which facilitated consistent and high-quality point cloud acquisition. The rRMSE for NQ was the lowest among the sites at 6.67%, further emphasizing the high precision achieved in this area. The results from NQ establish it as an optimal environment for the application of SLAM LiDAR for DBH estimation.

In the JQ site, the MAE increased slightly to 1.47 cm, while the rRMSE rose to 8.6%. The  $R^2$  value remained strong at 0.97, indicating reliable performance despite the slightly increased errors. The moderate canopy density and variation in tree spacing at this site may have introduced minor inconsistencies in point cloud density, which affected DBH estimation accuracy. Nonetheless, the results still demonstrated high reliability and supported the suitability of the SLAM LiDAR system for forest environments similar to JQ.

The JP site, characterized by dense and overlapping *Pinus densiflora* canopies, exhibited the highest errors, with an MAE of 1.89 cm and an rRMSE of 10.71%. Despite these increased errors, the  $R^2$  value at JP was still 0.97, indicating that the system maintained consistent performance even in complex forest environments. The denser canopy structure and overlapping branches in JP likely introduced shadowing effects and noise, which reduced the accuracy of the point cloud data around the DBH measurement height.

Aggregated across all three sites and 180 trees, the overall MAE was 1.45 cm, with an rRMSE of 8.97%, and the  $R^2$  value was 0.98. The maximum absolute error observed was 4.35 cm. These results validate the robustness of the SLAM LiDAR system for DBH estimation across diverse forest environments, with varying canopy structures and terrain complexities ([Figure 4](#)).

#### 3.2. DBH accuracy across size intervals

The accuracy of SLAM LiDAR-based DBH measurements was further analysed by grouping the results into five DBH size intervals: 0–10 cm, 10–20 cm, 20–30 cm, 30–40 cm, and  $\geq 40$  cm. The lowest class begins at 3 cm, the smallest diameter measured in the field. A one-way ANOVA on MAE confirmed that the five classes differed

**Table 2.** Validation of lidar-based DBH with field data.

Site	Count	MAE (cm)	MAPE (%)	RMSE (cm)	rRMSE (%)	$R^2$
NQ	60	1	9.03	1.26	6.67	0.99
JQ	60	1.47	12.84	1.85	8.6	0.97
JP	60	1.89	18.35	2.26	10.71	0.97
Overall	180	1.45	13.41	1.84	8.97	0.98

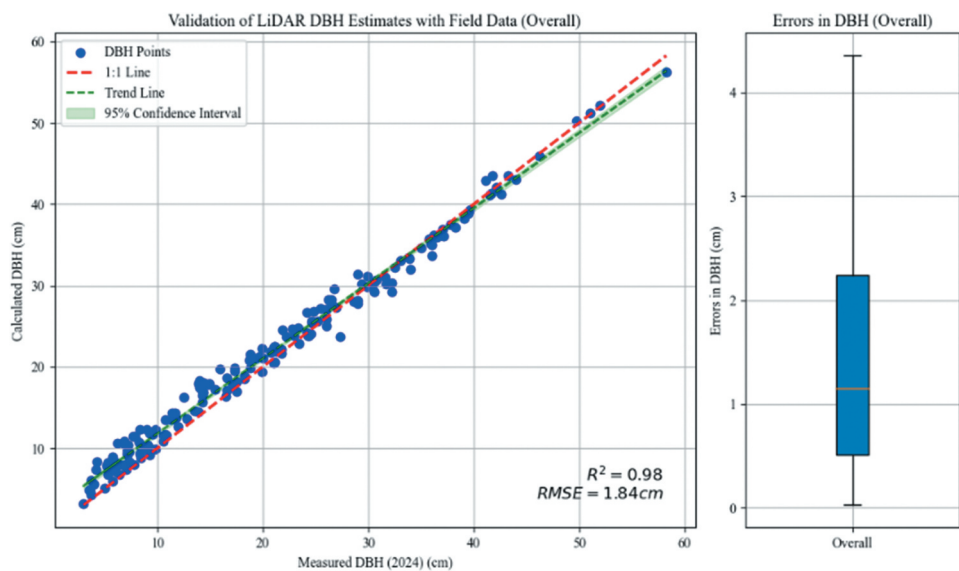


**Figure 4.** Comparison of DBH from field measurements and SLAM LiDAR. The overall  $R^2$  value of 0.98 demonstrates the strong alignment between the two measurement methods, with an average MAE of 1.45 cm and a maximum absolute error of 4.35 cm.

**Table 3.** Comparison of DBH results by 10 Cm intervals.

Interval	Count	MAE (cm)	MAPE (%)	RMSE (cm)	rRMSE (%)	$R^2$
0–10 cm	50	1.93	30.76	2.28	33.71	—
10–20 cm	44	1.88	13.23	2.2	14.72	0.43
20–30 cm	43	1.16	4.74	1.42	5.75	0.75
30–40 cm	30	0.76	2.22	1.05	3.03	0.87
≥40 cm	13	0.77	1.7	1.02	2.23	0.96

\*One-way ANOVA on MAE:  $F_{4,175} = 8.32$ ,  $p < 0.001$ .  
\* $R^2$  was not reported for 0–10 cm because total variance (SST) is too small for a meaningful coefficient of determination.  
Notes: The first class covers  $3 \leq \text{DBH} < 10$  cm (the smallest stem measured was 3 cm).

significantly ( $F_{4,175} = 8.32$ ,  $p < 0.001$ ). Table 3 provides a detailed summary of error metrics for each interval, including MAE, MAPE, RMSE, rRMSE, and  $R^2$  ( $R^2$  is not reported for the 0–10 cm class). The analysis revealed significant differences in measurement accuracy based on tree size.

For trees with DBH less than 10 cm, the highest errors were observed, with an MAE of 1.93 cm, a MAPE of 30.76%, and an rRMSE of 33.71%. These elevated errors were primarily due to the smaller surface area of thinner trunks, which limited the number of LiDAR point cloud returns available for DBH modelling. Additionally, the lower data density increased sensitivity to noise, resulting in reduced precision in cylinder fitting. In this class,  $R^2$  was effectively zero, indicating that a linear relationship between LiDAR- and caliper-derived DBH could not be established; MAE and MAPE therefore provide a more meaningful accuracy indicator for stems < 10 cm.

As tree size increased, accuracy improved significantly. For the 10–20 cm interval, the MAE decreased to 1.88 cm, and the MAPE dropped to 13.23%. The rRMSE

also declined to 14.72%, reflecting more reliable DBH measurements in this size range. In the 20–30 cm category, the MAE decreased further to 1.16 cm, while the MAPE and rRMSE were reduced to 4.74% and 5.75%, respectively. The  $R^2$  value increased to 0.75, showing better alignment between LiDAR-derived and manual measurements for medium-sized trees.

For trees in the 30–40 cm DBH range, the MAE reached its lowest at 0.76 cm, while the MAPE dropped to 2.22% and the rRMSE to 3.03%. The  $R^2$  value rose to 0.87, reflecting a high degree of precision in this category. Similarly, for trees with DBH  $\geq 40$  cm, the system achieved its best performance, with an MAE of 0.77 cm, a MAPE of 1.7%, and an rRMSE of 2.23%. The  $R^2$  value peaked at 0.96, indicating excellent alignment between the two measurement methods. These results suggest that the increased trunk surface area in larger trees provided denser point cloud data, enabling the LiDAR system to achieve greater accuracy in modelling DBH.

A locally weighted scatter-plot smoothing (LOWESS) analysis of absolute DBH errors indicated that the derivative of the fitted curve ( $|dy/dx|$ ) fell below 0.02 within a broad stability zone; the median diameter of this zone, 23.5 cm, was therefore adopted as the stability threshold. Above 23.5 cm the MAE remained  $< 1$  cm and the MAPE  $< 5\%$ , confirming that SLAM LiDAR yields consistently accurate DBH estimates for medium- and large-diameter trees (as illustrated in Figure 5(a,b)).

### 3.3. Variation in species composition and structural traits across DBH-based HDR classes

The composition of species and their structural characteristics varied across DBH classes, and a total of 31 species were recorded across all sites. In the small DBH class (0–10 cm), a total of 15 species were recorded across all survey sites. At the NQ site, *Acer*

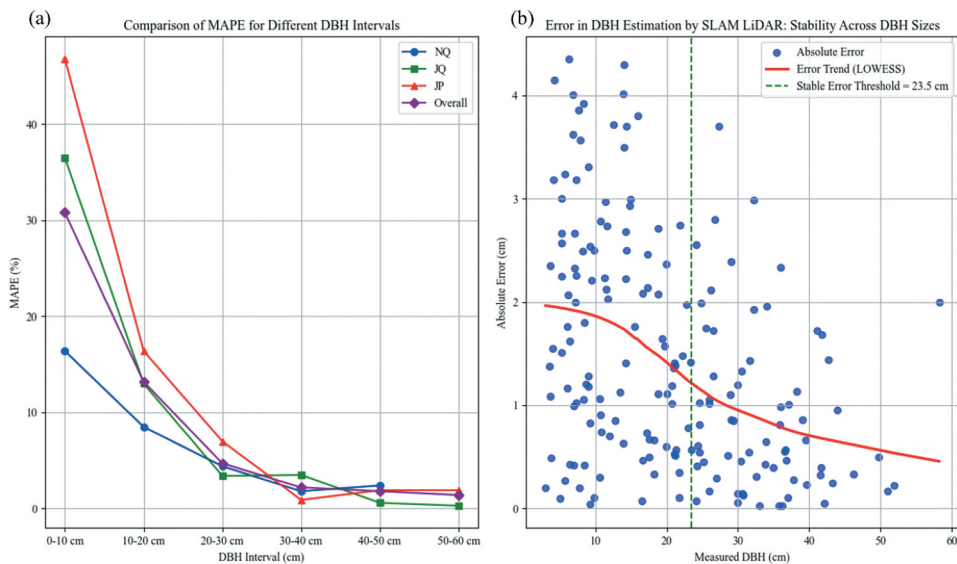


**Figure 5.** (a) Mean absolute percentage error (MAPE) for successive 10 cm DBH intervals. (b) Absolute error versus measured DBH with LOWESS trend (red) and the median stability threshold of 23.5 cm (green dashed line) derived from the  $|dy/dx| < 0.02$  criterion.

*pseudosieboldianum* and *Styrax japonicus* were dominant, accounting for over 50% of individuals. Conversely, the JQ and JP sites demonstrated a more balanced distribution of species, without a clear dominant species. In the medium DBH class (10–30 cm), a total of 23 species (DBH 10–20 cm: 19 species, DBH 20–30 cm: 13 species) were recorded across all survey sites. *Quercus mongolica* was dominant in both NQ and JQ, while JP showed co-dominance of *Q. mongolica* and *Quercus serrata*, suggesting an ongoing successional trend towards *Quercus*-dominated forest structure. In the large DBH class (> 30 cm), a total of 9 species (DBH 30–40 cm: 7 species, DBH > 40 cm: 5 species) were recorded across all survey sites. *Q. mongolica* remained dominant in NQ and JQ, while *Pinus densiflora* was the most prevalent species in JP, possibly reflecting site-specific differences in past disturbances or environmental conditions.

To examine whether DBH classes reflect differences in growth form, the HDR was calculated and compared across DBH groups.

The HDR exhibited a gradual decline in response to increasing DBH across all sites. The one-way analysis of variance (ANOVA) revealed statistically significant differences in the HDR among different DBH groups ( $F = 0.4334$ ,  $p < 0.005$ ). This indicates that while tree height remained relatively stable, an increase in DBH was the primary factor driving HDR variation (Figure 6). The results indicate that trees with smaller DBH exhibit substantially higher HDR values, implying a disproportionate allocation of growth to vertical rather than radial development. Given the relatively stable median tree heights across DBH classes, the observed variation in HDR is primarily attributable to differences in stem diameter. This pattern reflects a structural shift in growth strategy, whereby larger trees tend to allocate more resources to radial expansion than to vertical elongation. Such a shift may result from reduced competitive pressure or a diminished need for mechanical stabilization.

## 4. Discussion

### 4.1. Environmental influences on LiDAR-Derived DBH accuracy

The results demonstrated notable differences in DBH measurement accuracy across the three study sites, emphasizing the influence of ecological and structural conditions on

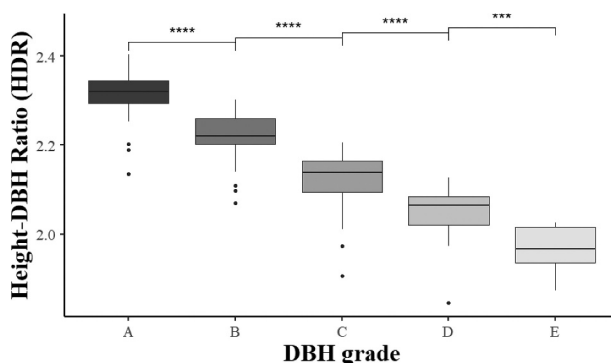


**Figure 6.** Boxplot comparing height-DBH ratio (HDR) across DBH grades. DBH grade categories: a (0–10 cm), B (10–20 cm), C (20–30 cm), D (30–40 cm), E (>40 cm) intervals. Significant differences were found between all groups (\*\*\*:  $p < 0.001$ , \*\*\*\*:  $p < 0.0001$ ).



SLAM LiDAR performance. The NQ site exhibited the highest accuracy, with an MAE of 1.0 cm and an  $R^2$  of 0.99, indicating precise alignment between LiDAR-derived and manual DBH measurements. This superior performance can be attributed to the relatively uniform canopy structure and minimal undergrowth in the NQ site, which facilitated consistent point cloud density around tree trunks and reduced variability in data quality. The open canopy layers and sparse understory at NQ likely minimized occlusion, allowing the LiDAR sensor to capture a clearer, more complete view of each tree's trunk (Zou et al. 2021). Additionally, uniform tree spacing in this site appears to have reduced overlapping signals, yielding cleaner returns and more reliable data for the cylinder-fitting algorithm.

In contrast, the JP site, with its dense *Pinus densiflora* canopy and overlapping branches, exhibited slightly higher errors, including an MAE of 1.89 cm and an rRMSE of 10.71%. The increased structural complexity in this site likely contributed to shadowing effects and reduced point cloud returns near the DBH measurement height, thereby introducing greater variability in the cylinder-fitting algorithm's outputs. Dense foliage can scatter or absorb the LiDAR beams, leading to partial or missing returns – especially around trunk areas that are overshadowed by foliage. Furthermore, fallen branches and thick understory vegetation at JP may also have contributed to data 'noise', which interferes with the segmentation of trunk points.

Similarly, the JQ site showed intermediate performance, with an MAE of 1.47 cm and an rRMSE of 8.6%, reflecting the influence of moderate canopy density and undergrowth conditions. Compared to JP, the canopy in JQ is slightly less dense, allowing for a higher proportion of successful trunk returns, yet still presenting enough structural variation to introduce some measurement errors. These site-specific variations highlight the relationship between forest structure and the accuracy of LiDAR-derived DBH measurements, demonstrating that environmental factors play a critical role in determining measurement reliability (Jakubowski, Guo, and Kelly 2013). For instance, differences in foliage density, tree spacing, understory vegetation height, and even topography can all contribute to variations in LiDAR performance. Overall, these findings suggest that while SLAM LiDAR is broadly effective in diverse forest settings, areas with uniform canopy structures and minimal undergrowth tend to offer the most favourable conditions for accurate DBH estimation. In more complex stands, targeted scanning strategies, higher-resolution sensors, or multi-sensor approaches may be necessary to minimize data loss and ensure reliable diameter measurements.

#### **4.2. Size class effects on DBH accuracy**

The accuracy of SLAM LiDAR-based DBH measurements varied significantly across different DBH size intervals. Trees with smaller DBH values – particularly those less than 10 cm – exhibited the highest errors, with a MAPE of 30.76% and an rRMSE of 33.71%. Overall agreement between LiDAR-derived and manual DBH was high ( $R^2 = 0.98$ , RMSE = 1.84 cm, MAE = 1.45 cm, maximum error = 4.35 cm). This elevated error rate can be partly attributed to the limited surface area of small trunks, which generate fewer LiDAR point cloud returns and thus undermine the reliability of the cylinder-fitting algorithm. Smaller trees are also more likely to be partially or completely occluded by understory vegetation or larger neighbouring trees, creating blind spots that reduce the number of valid returns at the DBH measurement height (Krůček et al. 2020). Moreover, the scanning geometry in

SLAM LiDAR surveys can be unfavourable for narrow stems; the laser beams may not intersect enough of the trunk's circumference to provide an adequate fit. Collectively, these factors lead to a sparser, noisier point cloud for small stems, making it challenging to accurately model their geometry.

Figure 7 underscores the importance of point count by showing a moderate correlation ( $R^2 = 0.544$ ) between DBH and point count. As DBH increases, the number of LiDAR returns also tends to rise, primarily due to the larger cross-sectional area of bigger trunks and more favourable laser incidence angles. In the smaller DBH classes where point counts are inevitably lower, error metrics (such as MAE and RMSE) typically increase. This pattern suggests that a critical minimum point count is necessary to achieve robust cylinder-fitting (Raguram, Frahm, and Pollefeys 2008). Without sufficient data, the algorithm may converge on incorrect trunk dimensions, amplifying errors in diameter estimation.

For trees with larger DBH values, error metrics improved consistently. Trees in the 30–40 cm DBH range achieved an MAE of 0.76 cm, reflecting a substantial reduction in measurement discrepancies compared to smaller classes. Meanwhile, trees with DBH values of 40 cm or more attained the highest accuracy, with an  $R^2$  of 0.96 and markedly lower error rates. The denser and more reliable point cloud data generated by thicker trunks provide the LiDAR system with abundant spatial information for modelling the tree circumference. Additionally, these larger trunks are less susceptible to partial occlusion, reducing the possibility of blind spots and incomplete data capture.

The identification of a stable error threshold at 23.5 cm further supports the notion that once tree diameter surpasses a certain range, the system delivers reliable and consistent DBH estimates. Beyond this threshold, diminishing errors suggest that the SLAM LiDAR's cylinder-fitting approach can effectively handle larger, more consistently measured

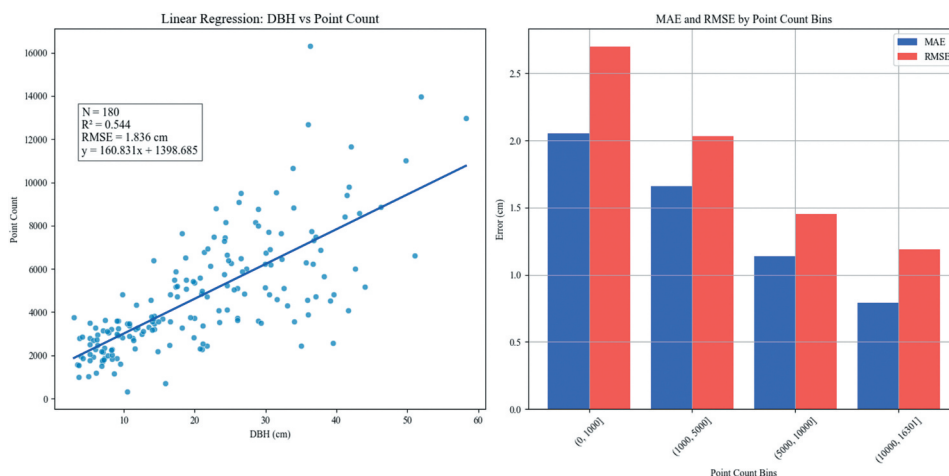


**Figure 7.** Relationship between DBH and LiDAR-derived point count, along with the mean absolute error (MAE) and root mean square error (RMSE) distribution across different point count bins. The left panel presents a linear regression model, demonstrating a moderate correlation ( $R^2 = 0.544$ ) between DBH and point count, with point count generally increasing as DBH increases. The right panel illustrates the error distribution, showing that as DBH increases, both MAE and RMSE tend to decrease, indicating improved accuracy in larger DBH measurements.

trunks. In practical terms, this implies that SLAM LiDAR is particularly well-suited for monitoring medium and large-sized trees in a variety of forest contexts. These trees not only benefit from increased point counts but also experience fewer occlusion effects, facilitating greater accuracy in point cloud generation.

Nevertheless, the higher error rates observed for smaller DBH classes should not be overlooked. In young or regenerating stands dominated by smaller trees, additional measures – such as adjusting scanning trajectories to capture trunks from multiple angles or employing higher-resolution LiDAR sensors – may be necessary to mitigate data scarcity. Future research could focus on optimizing scanning paths or integrating complementary sensing modalities to enhance coverage and improve DBH estimation accuracy for smaller stems. Despite these challenges, the present findings collectively reinforce the overall suitability of SLAM LiDAR for forest inventory applications, particularly when the aim is to monitor a broad range of size classes and ensure high accuracy for medium to large trees.

#### ***4.3. Species-specific structural traits and their influence on DBH measurement error***

Variation in HDR can be influenced by differences in stem growth patterns related to species-specific growth characteristics and responses to external environmental factors. Shade-tolerant species such as *Acer pseudosieboldianum* and *Styrax japonicus*, which often have curved stems, showed greater variability, whereas canopy-dominant *Quercus mongolica* and *Pinus densiflora* displayed uniform growth and lower error. In particular, high HDRs show a growth pattern with more vertical growth instead of volumetric growth, which is likely due to disruption from external environmental factors. Measurement discrepancies in DBH were notably pronounced in smaller trees (under 10 cm DBH), likely due to the smaller number of points in the point cloud and competitive growth effects. This observation underscores the complexity of how competitive growth shapes tree morphology and may impact measurement accuracy.

Similar limitations in measuring small-diameter trees have been discussed in previous studies. For instance, Li et al. (2020) reported a tendency for increased DBH estimation errors in trees with diameters under 10 cm when using SLAM-based LiDAR systems. Gonzalez-Benecke et al. (2021) also noted that measurement precision varied with crown coverage and neighbouring tree competition. Additionally, Calders et al. (2015) highlighted that automatic DBH retrieval tends to suffer from structural distortions in trees with lower point density. These findings are consistent with the results of this study, emphasizing the inherent challenges in accurately estimating DBH for small-diameter stems.

While many studies attribute the limitations in measuring small-diameter trees to insufficient point density, the underlying causes of this sparsity require closer examination. In this study, ANOVA tests for both DBH absolute error and error ratio across DBH classes revealed significant differences. According to Tukey's HSD post-hoc test, the absolute error was unexpectedly higher in Class B than in Class A trees (the thinnest class), with no statistically significant differences observed between Class A and Classes C, D, and E. In contrast, the error ratio decreased clearly with increasing DBH size: Class

**Table 4.** ANOVA results for DBH absolute error and error ratio by DBH class.

Response Variable	Df	Sum Sq	Mean Sq	F value	p value
Absolute Error(cm)	4	47.65	11.414	11.16	$p < 0.001$ ***
Error Ratio(%)	4	8610	2152.4	31.33	$p < 0.001$ ***

Notes: Asterisks indicate levels of statistical significance: \* $p < 0.05$ , \*\* $p < 0.01$ , \*\*\* :  $p < 0.001$ .

**Table 5.** Tukey HSD summary for DBH absolute error and error ratio by DBH class.

Variable	Tukey Grouping by DBH Class	Significant Groups
Absolute Error(cm)	B (a) > A (ab) > C (bc) > D = E (c)	B-A*, D-A*, C-B***, D-B***, E-B***
Error Ratio (%)	A (a) > B (ab) > C (bc) > D = E (c)	C-A***, D-A***, E-A***, C-B***, D-B***, E-B***

Notes: DBH grade categories: A (0–10 cm), B (10–20 cm), C (20–30 cm), D (30–40 cm), E (>40 cm) intervals. Different lowercase letters (a,b,c) indicate statistically significant differences among DBH class. Asterisks indicate levels of statistical significance: \* $p < 0.05$ , \*\* $p < 0.01$ , \*\*\* :  $p < 0.001$ .

A differed significantly from Classes C, D, and E, and even Class B differed significantly from Classes D and E (Tables 4, 5).

We particularly highlight the discrepancy in the results: although Class B trees exhibited higher absolute error than the thinner Class A trees, error ratio revealed significant differences between Class A and trees thicker than Class C. The absolute DBH error ranged from 0.04 to 4.3 cm, with maxima of 4.15 cm in Class A and 2.0 cm in Class E.

This variation reflects not only environmental noise but also intrinsic species-specific traits – such as bark roughness and non-linear stem form – that influence geometric reconstruction.

In particular, high HDR values in Class A suggest vertically biased growth under competitive light conditions, often resulting in curved or leaning stems that exacerbate measurement error. These discrepancies in small-diameter trees are likely due to the limited number of LiDAR points captured and the stronger influence of competitive growth, as non-upright stems can introduce errors in both LiDAR and manual measurements. While such traits can occur in larger trees, their relative impact on DBH accuracy is minor due to greater stem diameter and point cloud density. In smaller trees, however, even slight deviations can yield disproportionately high error ratios.

Several previous studies have indicated that sparse point returns and increased measurement errors may result from individual-level structural characteristics, such as leaning stems or crown asymmetry. For instance, in coniferous forests, some understory trees are more likely to experience occlusion and segmentation failure due to structural complexity and canopy shading (Brunner and Houtmeyers 2022). Additionally, Hamraz, Contreras, and Zhang (2016) noted that low point density in the understory layer of small-footprint airborne LiDAR often hampers accurate segmentation. These observations are consistent with our findings: individuals with higher error ratios were often shade-tolerant species, suggesting that shade-induced morphological plasticity may play a significant role in both point sparsity and DBH measurement error in LiDAR-based approaches.

Shade-tolerant species such as *A. pseudosieboldianum*, *S. japonicus*, *Q. serrata*, and *Fraxinus rhynchophylla*, observed in NQ and JQ, are typically late-successional, often growing under canopy pressure with limited light availability and competition for resources (Choung et al. 2020; Kim, Kang, and Lim 2016; Lei and Lechowicz 1990; Lienard, Harrison, and Gnanadesikan 2015). These conditions often result in leaning or

curved growth forms rather than upright stems (Saha, Kuehne, and Bauhus 2014). Similarly, shrub and sub-tree species including *Symplocos chinensis* var. *leucocarpa*, *Maackia amurensis*, *Salix gracilistyla*, and *Sorbus alnifolia*, observed in the JP forest, often exhibit non-vertical or curved stems due to external environmental factors, similar to those affecting shade-tolerant species (Sun, Liang, and Zhu 2021).

These non-upright growth patterns in thin trees may have contributed to discrepancies in LiDAR measurements, as non-upright stems can introduce errors in both LiDAR and manual measurements. The advantages of LiDAR lie in its ability to detect small trees and the significantly higher number of trees it can detect per unit of time compared to manual measurement, making it a valuable tool for forest assessments. While SLAM LiDAR requires improved accuracy for smaller trees, it remains effective for estimating understorey layers, including late-successional shrub and sub-tree species. In line with our size-class analysis, an operational threshold of approximately 23.5 cm was observed; beyond this threshold, DBH estimates were generally more stable and consistent across the study sites. This capability, essential for monitoring forest structure and succession, helps predict future vegetation dynamics, making LiDAR a valuable tool for long-term forest research and management.

## 5. Conclusion

This study examined the performance of a SLAM LiDAR system for measuring DBH across three forest sites (NQ, JP, and JQ) characterized by varying canopy structures and species compositions. Overall, LiDAR-derived DBH values displayed strong concordance with field measurements, maintaining an  $R^2$  of 0.98. Notably, the site with relatively uniform canopy coverage and minimal understory (NQ) achieved the highest consistency, underscoring how simpler stand structures facilitate more reliable trunk detection and modelling. Conversely, in sites with denser canopies or overlapping foliage (e.g. JP), occlusion and irregular understory layers led to modestly increased estimation errors, illustrating the influence of stand complexity on LiDAR data capture.

Analysis by DBH class showed that larger trees typically yielded more accurate measurements, reflecting the denser point clouds and reduced occlusion associated with bigger trunks. In contrast, smaller stems (< 10 cm DBH) exhibited greater errors, largely due to limited surface area and fewer LiDAR returns. A key finding was that beyond a certain DBH threshold – around 23 cm – measurement reliability improved considerably.

Furthermore, our findings indicate that elevated DBH errors in small-diameter trees are not solely attributable to point cloud sparsity, but also to species-specific structural traits such as curved stems and high HDR values associated with shade-tolerant growth strategies. These characteristics, while occasionally present in larger trees, contribute disproportionately to relative error in slender stems, emphasizing the importance of incorporating ecological variability into algorithm design.

Despite these challenges in small-diameter classes, the overall results affirm the practical utility of SLAM LiDAR for rapid, large-scale forest assessments, particularly when focusing on medium- to large-sized trees. Future enhancements, such as refined scanning trajectories, increased sensor resolution, or algorithmic adjustments for morphological plasticity, could further improve measurement accuracy for small stems.

In addition, our study highlights the need for ongoing refinement in LiDAR data processing techniques. By optimizing field acquisition strategies and incorporating structural diversity into modelling approaches, future work can enhance the precision and ecological relevance of automated forest inventories, supporting long-term ecosystem monitoring and data-driven management practices.

## Acknowledgment

This work was supported by the National Institute of Ecology [grant number NIE-B-2024-02].

## Disclosure statement

No potential conflict of interest was reported by the author(s).

## ORCID

Kim Daeyeol  <http://orcid.org/0000-0002-2215-4700>

## References

- Aabeyir, R., B. Kyereh, and J. A. Anaba. 2020. "Allometric Models for Estimating Aboveground Biomass in the Tropical Woodlands of Ghana, West Africa." *Journal of Forest Research* 25 (4): 231–240.
- Aschoff, T., & Spiecker, H. (2004). Algorithms for the automatic detection of trees in laser scanner data. The International Archives of the Photogrammetry, *Remote Sensing and Spatial Information Sciences*, Vol. XXXVI, Part 8/W2, 71–75
- Baker, T. R., O. L. Phillips, Y. Malhi, S. Almeida, L. Arroyo, A. Di Fiore, . . . & N. Higuchi. 2004. "Variation in Wood Density Determines Spatial Patterns in Amazonian Forest Biomass." *Global Change Biology* 10 (5): 545–562.
- Balestra, M., Cabo, C., Murtiyoso, A., Vitali, A., Alvarez-Taboada, F., Cantero-Amiano, A., ... & Pierdicca, R. (2024). Advancing forest inventory: a comparative study of low-cost MLS lidar device with professional laser scanners. *International Archives of the Photogrammetry, Remote Sensing and Spatial Information Sciences*, 48, 9-15.
- Bienert, A., L. Georgi, M. Kunz, H. G. Maas, and G. Von Oheimb. 2018. "Comparison and Combination of Mobile and Terrestrial Laser Scanning for Natural Forest Inventories." *Forests* 9 (7): 395. <https://doi.org/10.3390/f9070395>.
- Brunner, A., & Houtmeyers, S. (2022). Segmentation of conifer tree crowns from terrestrial laser scanning point clouds in mixed stands of Scots pine and Norway spruce. *European Journal of Forest Research*, 141(5), 909–925. <https://doi.org/10.1007/s10342-022-01481-5>.
- Calders, K., G. Newnham, A. Burt, S. Murphy, P. Raumonon, M. Herold, and M. Kaasalainen. 2015. "Nondestructive Estimates of Above-Ground Biomass Using Terrestrial Laser Scanning." *Methods in Ecology and Evolution* 6 (2): 198–208.
- Choung, Y., J. Lee, S. Cho, and J. Noh. 2020. "Review on the Succession Process of Pinus densiflora Forests in South Korea: Progressive and Disturbance-Driven Succession." *Forest Ecology & Management* 44 (1): 1–17. <https://doi.org/10.1186/s41610-020-00157-8>.
- Compeán-Aguirre, J. L., P. M. López-Serrano, J. L. Silván-Cárdenas, C. A. Martínez-García-Moreno, D. J. Vega-Nieva, J. J. Corral-Rivas, and M. Pompa-García. 2024. "Evaluation of Two-Dimensional DBH Estimation Algorithms Using TLS." *Forests* 15 (11): 1964. <https://doi.org/10.3390/f15111964>.
- Gonzalez-Benecke, C. A., Y. Ge, H. Lee, and T. A. Martin. 2021. "Quantifying Forest Structure Using SLAM-Based LiDAR: Implications for Biomass Estimation." *Remote Sensing* 13 (3): 512.



- Guan, T., Y. Shen, Y. Wang, P. Zhang, R. Wang, and F. Yan. 2024. "Advancing Forest Plot Surveys: A Comparative Study of Visual vs." *LIDAR SLAM Technologies Forests* 15 (12): 2083. <https://doi.org/10.3390/f15122083>.
- Hamraz, H., Contreras, M. A., & Zhang, J. (2017). Vertical stratification of forest canopy for segmentation of understory trees within small-footprint airborne LiDAR point clouds. *ISPRS Journal of Photogrammetry and Remote Sensing*, 130, 385–392. <https://doi.org/10.1016/j.isprsjprs.2017.07.001>.
- HariPriya, G. S. 2002. "Biomass Carbon of Truncated Diameter Classes in Indian Forests." *Forest Ecology & Management* 168 (1–3): 1–13. [https://doi.org/10.1016/S0378-1127\(01\)00729-0](https://doi.org/10.1016/S0378-1127(01)00729-0).
- Huang, H., Z. Li, P. Gong, X. Cheng, N. Clinton, C. Cao, W. Ni, and L. Wang. 2011. "Automated Methods for Measuring DBH and Tree Heights with a Commercial Scanning LiDAR." *Photogrammetric Engineering & Remote Sensing* 77 (3): 219–227. <https://doi.org/10.14358/pers.77.3.219>.
- Jakubowski, M. K., Q. Guo, and M. Kelly. 2013. "Tradeoffs Between Lidar Pulse Density and Forest Measurement Accuracy." *Remote Sensing of Environment* 130:245–253. <https://doi.org/10.1016/J.RSE.2012.11.024>.
- Kim, J. H., S. K. Kang, and S. M. Lim. 2016. "Community Ecological Revaluation of Acer Pseudosieboldianum and Carpinus Cordata in the Natural Deciduous Forest." *Journal of Forest and Environmental Science* 32 (1): 74–81. <https://doi.org/10.7747/JFES.2016.32.1.74>.
- Kirby, K. R., and C. Potvin. 2007. "Variation in Carbon Storage Among Tree Species: Implications for the Management of a Small-Scale Carbon Sink Project." *Forest Ecology & Management* 246 (2–3): 208–221. <https://doi.org/10.1016/j.foreco.2007.03.072>.
- Krůček, M., K. Král, K. C. Cushman, A. Missarov, and J. R. Kellner. 2020. "Supervised Segmentation of Ultra-High-Density Drone LiDAR for Large-Area Mapping of Individual Trees." *Remote Sensing* 12 (19): 3260. <https://doi.org/10.3390/RS12193260>.
- Kurdi, F. T., E. Lewandowicz, J. Shan, and Z. Gharineiat. 2024. "Three-Dimensional Modeling and Visualization of Single Tree LiDAR Point Cloud Using Matrixial Form." *IEEE Journal of Selected Topics in Applied Earth Observations & Remote Sensing* 17:3010–3022. <https://doi.org/10.1109/JSTARS.2024.3349549>.
- Kuželka, K., and P. Surový. 2024. "Noise Analysis for Unbiased Tree Diameter Estimation from Personal Laser Scanning Data." *Remote Sensing* 16 (7): 1261. <https://doi.org/10.3390/rs16071261>.
- Lei, T. T., and M. J. Lechowicz. 1990. "Shade Adaptation and Shade Tolerance in Saplings of Three Acer Species from Eastern North America." *Oecologia* 84 (4): 224–228. <https://doi.org/10.1007/BF00318275>.
- Lee, T. B. (2003). *Coloured Flora of Korea*, Vols. I–II. Seoul: Hyangmunsa.
- Li, Y., Q. Sun, M. Li, and W. Zhang. 2020. "Individual Tree Diameter Measurement Using Handheld SLAM lidar in Forest Environments." *Forests* 11 (12): 1267.
- Lienard, J., S. P. Harrison, and A. Gnanadesikan. 2015. "An Appraisal of the Classic Forest Succession Paradigm with the Shade Tolerance Index." *PLOS ONE* 10 (4): e0124436.
- Liu, L., A. Zhang, S. Xiao, S. Hu, N. He, H. Pang, and S. Yang. 2021. "Single Tree Segmentation and Diameter at Breast Height Estimation with Mobile LiDAR." *IEEE Access* 9:24314–24325. <https://doi.org/10.1109/ACCESS.2021.3056562>.
- McRoberts, R. E., E. O. Tomppo, and E. Næsset. 2010. "Advances and Emerging Issues in National Forest Inventories." *Scandinavian Journal of Forest Research* 25 (4): 368–381. <https://doi.org/10.1080/02827581.2010.496739>.
- Morales, A., and D. W. MacFarlane. 2024. "Reducing Tree Volume Overestimation in Quantitative Structure Models Using Modeled Branch Topology and Direct Twig Measurements." *Forestry: An International Journal of Forest Research*, cpae046. 98 (3): 394–409. <https://doi.org/10.1093/forestry/cpae046>.
- Nalaka, G. D. A., T. Sivananthawerl, and M. C. M. Iqbal. 2013. "Scaling Aboveground Biomass from Small Diameter Trees." *Tropical Agricultural Research* 24 (2): 150–162.
- Nam, V. T., D. V. Tinh, A. Nizovtsev, H. N. Bao, D. T. Hung, and N. M. Ha. 2016. "Allometric Equations

- for Aboveground and Belowground Biomass Estimations in an Evergreen Forest in Vietnam." *Forest Ecosystems* 3 (1): 1–11.
- National Institute of Biological Resources. 2023. "National List of Species of Korea." Incheon, South Korea: National Institute of Biological Resources. <https://www.nibr.go.kr>.
- National Institute of Ecology. 2023. 2023 National Long Term Ecological Research in Korea. Report No. NIE-B-2023-02. National Institute of Ecology.
- Pang, C., L. Zhou, and X. Huang. 2024. "A Low-Cost 3D SLAM System Integration of Autonomous Exploration Based on Fast-ICP Enhanced Lidar-Inertial Odometry." *Remote Sensing* 16 (11): 1979. <https://doi.org/10.3390/rs16111979>.
- Parresol, B. R. 1999. "Assessing Tree and Stand Biomass: A Review with Examples and Critical Comparisons." *Forest Science* 45:573–593. <https://doi.org/10.1093/forestscience/45.4.573>.
- Pierzchała, M., P. Giguère, and R. Astrup. 2018. "Mapping Forests Using an Unmanned Ground Vehicle with 3D LiDAR and Graph-SLAM." *Computers and Electronics in Agriculture* 145:217–225. <https://doi.org/10.1016/j.compag.2017.12.034>.
- Raguram, R., J. M. Frahm, and M. Pollefeys. 2008. "A Comparative Analysis of RANSAC Techniques Leading to Adaptive Real-Time Random Sample Consensus." Computer Vision–ECCV 2008: 10th European Conference on Computer Vision, Marseille, France, October 12–18, 2008, Proceedings, Part II 10, Berlin Heidelberg.: 500–513. Springer.
- R Core Team. 2024. "R: A Language and Environment for Statistical Computing (Version 4.4.1)." [Computer Software.], R Foundation for Statistical Computing. <https://www.R-project.org/>.
- Saha, S., C. Kuehne, and J. Bauhus. 2014. "Intra- and Interspecific Competition Differently Influence Growth and Stem Quality of Young Oaks (*Quercus robur* L. and *Quercus petraea* (Mattuschka) Liebl.)." *Forest Ecology & Management* 324 (3): 105–115. <https://doi.org/10.1007/s13595-013-0345-1>.
- Salehi, B., S. Jarahizadeh, and A. Sarafraz. 2022. "An Improved RANSAC Outlier Rejection Method for UAV-Derived Point Cloud." *Remote Sensing* 14 (19): 4917. <https://doi.org/10.3390/rs14194917>.
- Schnabel, R., R. Wahl, and R. Klein. 2007. "Efficient RANSAC for Point-Cloud Shape Detection." *Computer Graphics Forum* 26 (2): 214–226. Oxford, UK: Blackwell Publishing Ltd. June. <https://doi.org/10.1111/j.1467-8659.2007.01016.x>.
- Shao, J., Zhang, W., Mellado, N., Wang, N., Jin, S., Cai, S., Luo, L., Lejemble, T., & Yan, G. (2020). SLAM-aided forest plot mapping combining terrestrial and mobile laser scanning. *ISPRS Journal of Photogrammetry and Remote Sensing*, 163(3), 214–230. <https://doi.org/10.1016/j.isprsjprs.2020.03.008>.
- Sun, S., Zhang, J., Zhou, J., Guan, C., Lei, S., Meng, P., & Yin, C. (2021). Long-term effects of climate and competition on radial growth, recovery, and resistance in Mongolian pines. *Frontiers in Plant Science*, 12, 729935. <https://doi.org/10.3389/fpls.2021.729935>.
- Tarsha Kurdi, F., Z. Gharineiat, E. Lewandowicz, and J. Shan. 2024. "Modeling the Geometry of Tree Trunks Using LiDAR Data." *Forests* 15 (2): 368. <https://doi.org/10.3390/f15020368>.
- Tomppo, E., T. Gschwantner, M. Lawrence, R. E. McRoberts, K. Gabler, K. Schadauer, and E. Cienciala. 2010. "National Forest Inventories. Pathways for Common Reporting." *European Science Foundation* 1:541–553. <https://doi.org/10.1007/978-90-481-3233-1>.
- Xie, Y., T. Yang, X. Wang, X. Chen, S. Pang, J. Hu, and A. Wang, L. Chen, Z. Shen. 2022. "Applying a Portable Backpack lidar to Measure and Locate Trees in a Nature Forest Plot: Accuracy and Error Analyses." *Remote Sensing* 14 (8): 1806. <https://doi.org/10.3390/rs14081806>.
- Xie, Y., J. Zhang, X. Chen, S. Pang, H. Zeng, and Z. Shen. 2020. "Accuracy Assessment and Error Analysis for Diameter at Breast Height Measurement of Trees Obtained Using a Novel Backpack lidar System." *Forest Ecosystems* 7:1–11. <https://doi.org/10.1186/s40663-020-00237-0>.
- Yang, S., Y. Xing, D. Wang, and H. Deng. 2024. "A Novel Point Cloud Adaptive Filtering Algorithm for LiDAR SLAM in Forest Environments Based on Guidance Information." *Remote Sensing* 16 (15): 2714. <https://doi.org/10.3390/rs16152714>.
- Yao, W., P. Krzystek, and M. Heurich. 2012. "Tree Species Classification and Estimation of Stem Volume and DBH Based on Single Tree Extraction by Exploiting Airborne Full-Waveform LiDAR Data." *Remote Sensing of Environment* 123:368–380. <https://doi.org/10.1016/j.rse.2012.03.027>.

- Ye, W., C. Qian, J. Tang, H. Liu, X. Fan, X. Liang, and H. Zhang. 2020. "Improved 3D Stem Mapping Method and Elliptic Hypothesis-Based DBH Estimation from Terrestrial Laser Scanning Data." *Remote Sensing* 12 (3): 352. <https://doi.org/10.3390/rs12030352>.
- Zhang, W., J. Qi, P. Wan, H. Wang, D. Xie, X. Wang, and G. Yan. 2016. "An Easy-to-Use Airborne LiDAR Data Filtering Method Based on Cloth Simulation." *Remote Sensing* 8 (6): 501. <https://doi.org/10.3390/rs8060501>.
- Zhao, K., S. C. Popescu, and R. Nelson. 2009. "Lidar Remote Sensing of Forest Biomass: A Scale-Invariant Estimation Approach Using Airborne Lasers." *Remote Sensing of Environment* 113 (1): 182–196. <https://doi.org/10.1016/J.RSE.2008.09.009>.
- Zhou, Z., D. M. Meneses, Y. Yu, J. Gong, and Q. Guo. 2021. "Delineation of Small Flat Watershed with High-Resolution DEM from Terrestrial Laser Scanning." *Journal of Hydrologic Engineering* 26 (7): 04021021. [https://doi.org/10.1061/\(ASCE\)HE.1943-5584.0002096](https://doi.org/10.1061/(ASCE)HE.1943-5584.0002096).
- Zou, Q., Q. Sun, L. Chen, B. Nie, and Q. Li. 2021. "A Comparative Analysis of LiDAR SLAM-Based Indoor Navigation for Autonomous Vehicles." *IEEE Transactions on Intelligent Transportation Systems* 23 (7): 6907–6921. <https://doi.org/10.1109/TITS.2021.3063477>.